Structure
Article

Structure of Osh3 Reveals a Conserved Mode of Phosphoinositide Binding in Oxysterol-Binding Proteins

Junsen Tong,[1] Huiseon Yang,[1] Hongyuan Yang,[2] Soo Hyun Eom,[3] and Young Jun Im[1,*]
[1]College of Pharmacy, Chonnam National University, Gwangju 500-757, South Korea
[2]School of Biotechnology and Biomolecular Sciences, The University of New South Wales, Sydney, New South Wales 2052, Australia
[3]Department of Life Science, Gwangju Institute of Science and Technology, Gwangju 500-712, South Korea
*Correspondence: imyoungjun@jnu.ac.kr
http://dx.doi.org/10.1016/j.str.2013.05.007

SUMMARY

The oxysterol-binding protein (OSBP)-related proteins (ORPs) are conserved from yeast to humans, and implicated in the regulation of lipid homeostasis and in signaling pathways. *Saccharomyces cerevisiae* has seven ORPs (Osh1–Osh7) that share one unknown essential function. Here, we report the 1.5–2.3 Å structures of the PH domain and ORD (OSBP-related domain) of yeast Osh3 in apo-form or in complex with phosphatidylinositol 4-phosphate (PI[4]P). Osh3 recognizes PI(4)P by the highly conserved residues in the tunnel of ORD whereas it lacks sterol binding due to the narrow hydrophobic tunnel. Yeast complementation tests suggest that PI(4)P binding to PH and ORD is essential for function. This study suggests that the unifying feature in all ORP homologs is the binding of PI(4)P to ORD and sterol binding is additional to certain homologs. Structural modeling of full-length Osh3 is consistent with the concept that Osh3 is a lipid transfer protein or regulator in membrane contact sites.

INTRODUCTION

Oxysterol-binding proteins (OSBP)-related proteins (ORPs) constitute a large and evolutionarily conserved family of lipid-binding proteins in the eukaryotic kingdom. They are implicated in many cellular processes including cell signaling, vesicular trafficking, lipid metabolism, and nonvesicular sterol transport (Beh et al., 2012; Raychaudhuri and Prinz, 2010). The budding yeast has seven ORP genes, *OSH1–OSH7*. Humans have 12 ORP genes and splicing variations of these genes increase the number of different protein products (Lehto et al., 2001). A common feature for all ORPs is the conserved C-terminal OSBP-related domain (ORD). ORDs of several ORPs were known to bind sterols (Ngo et al., 2010) and Osh4 binds phosphatidylinositol 4-phosphate (PI[4]P) in the partly overlapping binding pocket with sterol (de Saint-Jean et al., 2011). ORPs can be divided into two subtypes, "long" and "short" homologs. Short ORPs comprise only an ORD with little additional sequences. Long ORPs contain additional N-terminal variable regions such as pleckstrin homology (PH) domains, endoplasmic reticulum (ER)-targeting FFAT (two phenylalanines in an acidic tract) motifs, transmembrane regions, GOLD (Golgi dynamics) domains, and/or ankyrin repeats. These additional domains localize ORPs by binding to phosphoinositides (Levine and Munro, 2001; Ngo et al., 2010), the ER protein VAP (vesicle-associated membrane protein [VAMP]-associated protein; Loewen et al., 2003), and other targeting signals.

Sterols are essential membrane components that constitute ~30%–40% of plasma membrane (PM) lipids (Mesmin and Maxfield, 2009). Sterols are synthesized in the ER and rapidly transported to the PM (Baumann et al., 2005). Because sterols are water insoluble, their nonvesicular transport between membranes is predicted to require lipid transfer proteins (LTPs) (Mesmin et al., 2013). ORPs are potential candidates for LTPs that extract a sterol from a donor membrane to a shielded pocket and transfer the sterol to an acceptor membrane (Beh et al., 2012). Both long and short ORPs can be enriched at membrane contact sites, where they are suggested to execute regulatory or lipid transfer functions (Schulz et al., 2009; Vihervaara et al., 2011a). In addition to sterol ligands, Osh4 was shown to bind PI(4)P in the binding pocket and exchanges sterols for PI(4)P between lipid membranes (de Saint-Jean et al., 2011).

Besides the role as LTPs, diverse functions of ORPs have been reported as sterol regulators or sensors that relay information to a spectrum of different cellular processes (Beh et al., 2012). Human OSBP1 is a cholesterol-sensing regulator of two protein phosphatases affecting the phosphorylation status of ERK (Wang et al., 2005). ORP1L in complex with Rab7 GTPase and RILP regulates the distribution and motility of late endosomes (Vihervaara et al., 2011b). Oxysterol binding changes the subcellular localization of OSBP1, ORP1L, and ORP2, suggesting a sterol sensor action of these ORPs (Ridgway et al., 1992; Vihervaara et al., 2011a). ORPs are also implicated in a variety of other signaling pathways including, PKCβ/Akt signaling in mast cells (Lessmann et al., 2007), and Rho-mediated polarized cell growth in yeast (Kozminski et al., 2006). Several Oshs (Osh3–Osh7) act as controllers of PI(4)P signaling and metabolism by regulating Sac1 phosphatase at membrane contact sites (Stefan et al., 2011).

In budding yeast, deletion of all seven ORPs is lethal (Beh et al., 2001). In yeast strains lacking all but one *OSH* gene, gradual turning off of the last remaining Osh2 gene causes severe defects in sterol and lipid distribution (Beh and Rine, 2004). The expression of any single *OSH* gene averts this

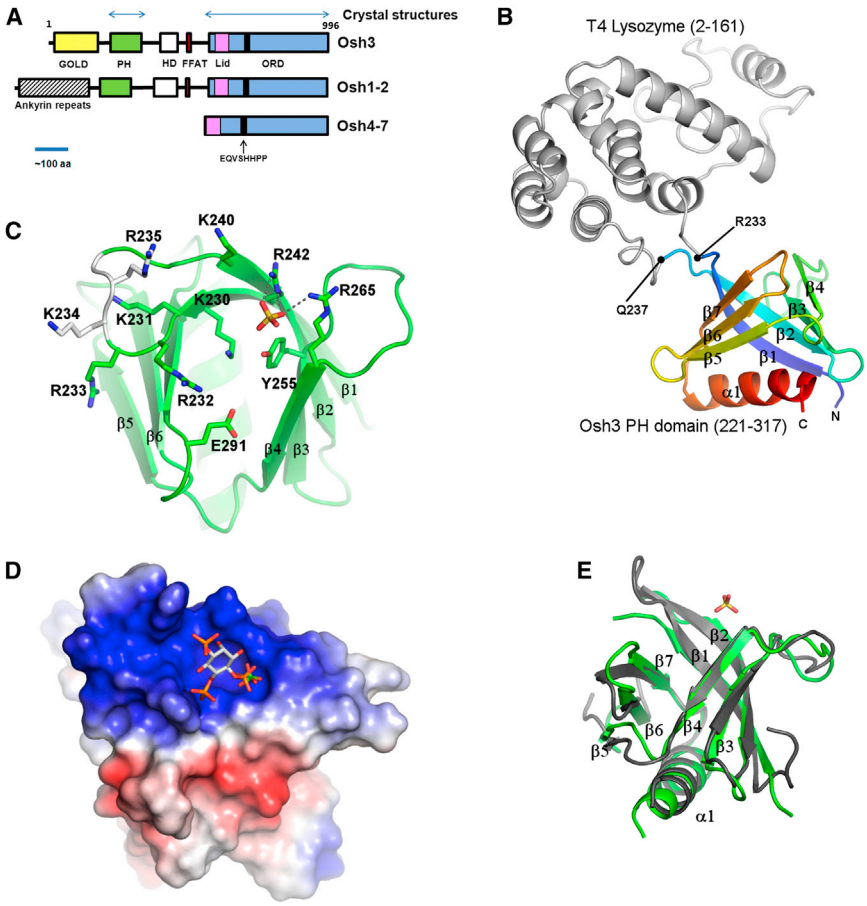

Figure 1. Structure of the Osh3 PH Domain

(A) Schematic representation of the domain structures of ORP homologs in yeast.

(B) The overall structure of the Osh3 PH-T4 lysozyme. The T4 lysozyme is shown in gray, and the PH domain is blue to red based on the secondary structure succession.

(C) Ribbon representation of the phosphoinositide binding pocket of the PH domain. The basic residues and the key residues in the binding pocket are shown as ball-and-stick models. The three peptides (residues 234–236) replaced by T4 lysozyme were modeled and are gray.

(D) Electrostatic surface representation of the PH domain. Ins(1,4,5)P_3 were modeled based on the superposition of the cytohesin-2 PH-IP_3 structure (PDB code 1U29). The sulfate ion bound to the Osh3 PH domain is shown as ball-and-stick models.

(E) Superposition of the Osh3 PH domain (green) and the human pleckstrin PH domain (gray).

See also Figures S1 and S2.

lethality, indicating that all Osh homologs share at least one essential function. The structure of a short yeast homolog Osh4 revealed that the protein core is an incomplete β barrel with a ligand-binding tunnel (Im et al., 2005). Osh4 binds a single molecule of lipid such as cholesterol, ergosterol, oxysterols, and PI(4)P to shield its hydrophobic acyl chains from the aqueous environment (de Saint-Jean et al., 2011; Im et al., 2005). Currently, Osh4 is the only ORP homolog with a known three-dimensional structure. Because the sequence homology of Osh4 to other long ORP members is low and the function of each ORP member is diverse, extrapolation of structural features of Osh4 to other ORPs is limited. Still, the ligand specificities of many ORPs and the mechanistic relationship between the N-terminal domains and the ORD are not known clearly. Most of all, the essential function shared by all ORPs remains elusive.

In this study, we determined the structures of the PH domain and ORD of Osh3, one of the long ORP members. We found that Osh3 completely lacks sterol binding activity while binding of PI(4)P to its ORD is essential for function. Structural analysis and modeling of full-length Osh3 is consistent with the role of Osh3 as an LTP or as a regulator at membrane contact sites. This study provides key evidence for the shared role of ORPs and redefines the major roles of ORPs as phosphoinositide binding proteins.

RESULTS

Structure of Osh3 PH

Osh3 contains a GOLD domain (residues 1–195) and PH domain (residues 222–317) in the N-terminal region. The middle region between the PH domain and ORD contains a predicted helical region (residues 460–500), and an FFAT motif (EFFDAEE, residues 514–520; Figure 1A). To overcome the poor solubility of the PH domain in *Escherichia coli* overexpression, we engineered a fusion protein (Osh3 PH-T4L) in which T4 lysozyme replaces three amino acids (residues 234–236) in the β1-β2 loop of Osh3 PH, which yielded soluble expression of the chimeric protein (Tong et al., 2012). The structure of Osh3 PH was determined at 2.3 Å resolution by molecular replacement using T4 lysozyme as a search model and the structure was refined to an R factor of 24.4% (Table 1). The final model contained two molecules of Osh3 PH-T4L, eight sulfate ions, and 106 water molecules in the asymmetric unit. The T4 lysozyme has an extended conformation from the PH domain with no intramolecular interaction between the PH and lysozyme except for a few residues in the linker (Figure 1B). The Osh3 PH displays a typical PH domain fold consisting of a seven-stranded antiparallel β sheet and a C-terminal amphipathic α-helix. One sulfate ion contained in the crystallization buffer is coordinated by the side chains of Arg242 (β2), Arg265 (β4), and Tyr255 (β3) in the canonical phosphoinositide binding site formed by the β1-β2 and β3-β4 loops (Figure 1C). Comparison of Osh3 PH with the Cytohesin-2 PH domain (Protein Data Bank [PDB] code 1U29) reveals that the sulfate ion occupies the position of the 4-phosphate in Ins(1,4,5)P_3 (Figure 1D). A total of ten positive residues are clustered in the phosphoinositide binding site (nine residues in the β1-β2 and one residue in the β3-β4 loops), contributing to the strong electropositive surface (Figure 1D). A previous genome-wide analysis of yeast PH domains indicated that Osh3 PH

Table 1. Statistics of Data Collection and Crystallographic Refinement

Crystal	PH-Lysozyme	Apo ORD (Br Derivative)	Apo ORD (Native Form)	ORD (PI(4)P Complex)
Wavelength (Å)	0.97949	0.91950 (peak)	0.91997	0.97949
X-ray source	5C, PLS	AR-NW12A, PF	BL17U1, SSRF	5C, PLS
Space group	C2	$P2_12_12_1$	$P2_12_12_1$	$P2_12_12_1$
Unit cell (Å)	a = 98.0, b = 91.3, c = 84.1	a = 40.9, b = 89.2, c = 96.1	a = 40.9, b = 89.2, c = 96.1	a = 39.9, b = 89.0, c = 95.7
Resolution (Å) (last shell)	2.3 (2.34–2.30)	1.9 (1.93–1.90)	1.5 (1.53–1.50)	2.2 (2.24–2.20)
No. of unique reflections	32,983	29,751	56,991	18,011
Redundancy	3.3 (3.0)	14.6 (14.8)	7.7 (5.9)	7.9 (8.1)
I/s(I)σ (last shell)	23.2 (3.5)	54.3 (12.8)	40.0 (4.6)	23.0 (5.3)
Rsym[a] (%)	6.7 (30.8)	7.0 (26.9)	8.8 (34.3)	10.7 (37.9)
Data completeness (%)	99.4 (98.7)	99.9 (100.0)	99.7 (99.4)	100.0 (100.0)
Phasing	MR	Br-SAD	–	MR
Mean FOM (50–1.9 Å)	–	0.34 (SOLVE)	–	–
Overall FOM (50–1.9 Å)	–	0.67 (RESOLVE)	–	–
Refinement	–	–	–	–
R factor (%)	24.4 (29.4)	–	21.3 (22.8)	23.2 (26.8)
Free R factor[a] (%)	27.6 (34.4)	–	23.9 (25.9)	28.0 (31.0)
Rms bond length (Å)	0.006	–	0.005	0.006
Rms bond angle (°)	1.2	–	1.3	1.3
Average B value (Å^2)	43.6	–	20.3	29.2
Number of atoms	4,285	–	3,331	3,199

The values in parentheses relate to highest-resolution shells.
[a]R_{free} is calculated for a randomly chosen 5% of reflections.

displays promiscuous binding to several types of phosphoinositides—PI(3)P, PI(4)P, PI(3,4)P_2, and PI(4,5)P_2—in lipid overlay assays (Yu et al., 2004). It is probable that the affinities of Osh3 PH to various PIPs could be mediated by conformational adaptation of the flexible β1-β2 loop containing five additional positive residues (residues 231–235) compared to canonical PH domains. Recent functional studies showed that Osh3 localizes to PM/ER contact sites in a PI(4)P-dependent manner and deletion of the Osh3 PH domain displayed increased cytoplasmic localization, suggesting that Osh3 PH recognizes PI(4)P or PI(4,5)P_2 in the PM (Stefan et al., 2011).

The structure of Osh3 PH shows a high structural similarity (root-mean-square deviation [rmsd] of 1.2 Å for equivalent 75 Cα atoms) to that of the human plecksrin PH domain (PDB code 2i5f), which displays 22% sequence identity to Osh3 PH (Figure 1E). Osh3 PH has 28%–32% sequence identity to the PH domains of other long ORP members (ORP3, ORP6, ORP7, ORP10, ORP11, ORP4, and OSBP1; Figure S1 available online). This observation suggests that the PH domains of these ORP members have a high degree of structural conservation. The key residues (Tyr255, Arg255, and Arg265) that recognize the 4-phosphate group of phosphoinositide are strictly conserved in these ORPs. In particular, the PH domains of Osh3, ORP3, ORP6, and ORP7 commonly have eight to nine positive residues in the β1-β2 loops, implying that they might share common ligand binding properties.

Structure of Osh3 ORD

The structure of Osh3 ORD was determined at 1.5 Å resolution by the single anomalous dispersion method using sodium bromide added in the crystallization solution (Table 1). The structure of Osh3 ORD displays a central ligand binding tunnel with a flexible lid covering the tunnel entrance (Figures 2A–2C). The core of Osh3 ORD is built around a central antiparallel β sheet of 19 strands that forms an incomplete β barrel. A tunnel with a volume of 1,511 Å^3 is located in the center of the barrel. The tunnel is flanked by an N-terminal domain (residues 662–723) and a large C-terminal region (residues 885–996). The N-terminal domain following the lid consists of a two-stranded β sheet and three α helices that form a 50 Å long antiparallel bundle. The large carboxyl terminal region following the barrel contains four α helices and two β strands forming a hairpin. Residues 641–661 form a lid covering the tunnel opening. The lid of Osh3 contains two turns of an amphipathic α helix. The upstream residues of the lid (residues 625–640) form an extended loop on the concave surface of the C-terminal region (Figure 2D).

The N-Terminal Lid of Osh3 ORD Has Limited Flexibility

Apo Osh3 ORD has a closed conformation of the lid by weak hydrophobic interactions between the lid and the entrance of the hydrophobic tunnel. The protruding tip of the lid (residues 649–657) is partially disordered with the highest *B*-factors in the structure (Figure 2E), suggesting that the flexible lid might allow the transition between open and closed conformations for ligand uptake and release. Upstream, 16 residues from the lid form an extended loop and make tight binding to the surface of the C-terminal domain of ORD (Figure 2D). The shallow pocket accommodating the upstream residues is composed of the β17-α7 and α7-α8 loops. Two conserved arginine residues (residues 629–630) make hydrogen bonds with Glu911 (α6-α7) and a salt

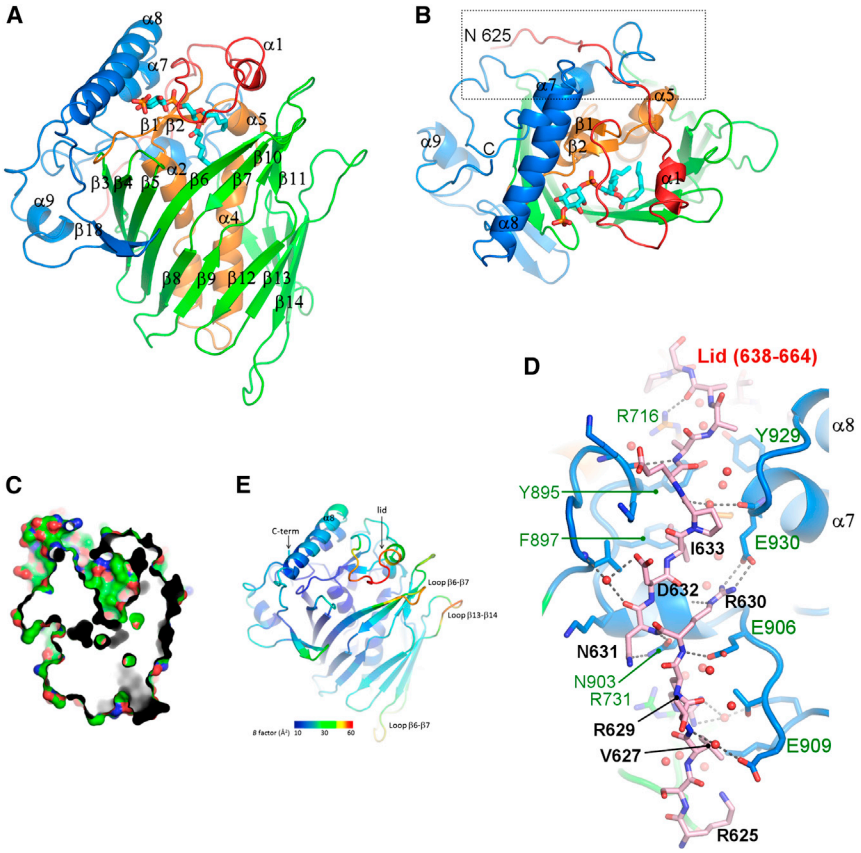

Figure 2. Structure of Osh3 ORD

(A) The overall structure of Osh3 ORD. The N-terminal lid (residues 641–661) is shown in red, the central helices (664–724) in orange, the β barrel (725–886) in green, and the C-terminal subdomain (887–996) in blue. Bound PI(4)P is shown as a stick model.

(B) Top view of Figure 2A. The N-terminal 15 residues marked by a dashed box are shown in detail in Figure 2D.

(C) The surface representation of Osh3 ORD. Basic residues are shown in blue, acidic residues in red, hydrophobic residues in green, and neutral polar residues in white.

(D) The N-terminal upstream residues of the lid. The N-terminal residues are pink and the labels are black. The residues interacting with the N-terminal residues are green.

(E) B-factor representation of apo Osh3 ORD.

bridge with Glu930 (α7) in the shallow pocket. Ile633 is accommodated in the hydrophobic pocket formed by helix α6 and the loop β17-α6. The strong interaction indicates that the upstream region of the lid is always associated with the β barrel regardless of conformational states of Osh3. This might serve as a stopper of tension from the N-terminal domains, allowing independent gating of the lid in ORD. The fixation of the N-terminal end of the lid in Osh3 contrasts sharply to the flexible end of the lid in Osh4. The N-terminal lid of Osh4 lacking the upstream residues is completely open and disordered when ligand is absent (Im et al., 2005). The fixation of the N-terminal lid observed in Osh3 seems common for many ORP members. The key binding motifs of (R/K)-(R/K)-X-X-I-(P/D) (residues 629–634) in the upstream residues are conserved in OSBP1, ORP2, ORP3, ORP4, ORP6, ORP7, and yeast Osh1–Osh3 (Figure S1).

Binding of PI(4)P to Osh3 ORD

The structure of the Osh3 ORD-PI(4)P complex was determined at 2.2 Å resolution by molecular replacement using the apo form (Table 1). The PI(4)P molecule is well ordered in the structure with a strong electron density map on the head group of the ligand (Figure S2). PI(4)P binds to Osh3 ORD by inserting two acyl chains into the central hydrophobic tunnel of the β barrel. The phosphoinositol group is accommodated by the shallow basic pocket in the tunnel entrance (Figures 3A and 3B). The conserved residues Lys941, Arg949, Arg952, and Glu945 from helix α8 undergo conformational adjustments of side chains to make direct interaction with the polar phosphoinositol group. The acyl chains of PI(4)P interact loosely with the hydrophobic tunnel in a rather nonspecific manner, as suggested by the weak electron density observed for this part of the ligand. In contrast, the polar inositol head group is involved in many direct and water-mediated interactions with the protein, accounting for the specific recognition of PI(4)P by Osh3 ORD. The 4-phosphate group forms direct hydrogen bonds with the side chains of His745, Arg746 (β4-β5), and Arg949 (α8), and water-mediated interactions with Arg949 (α8) and Glu945 (α8). The 1-phosphate group bridging the inositol ring and the glycerol moiety is hydrogen-bonded to Lys717 (β2) and Asn720 (β2) and the backbone amide of Met660 in the lid (Figure 3A). The 4-hydroxyl group of the inositol ring forms a direct hydrogen bond with Glu945 (α8), and the 3-hydroxyl group is involved in water-mediated interaction with the backbone carbonyl oxygen of Glu945. Molecular modeling suggested that Osh3 ORD could not bind PI(4,5)P_2 because the 5-phosphate group causes a steric clash with the side chains of Glu948 and His745. A 3-phosphate group also seems unfavorable due to the steric hindrance with the backbone of Ser657 and Ile658 of the lid. The hydrogen bonding network of the phosphoinositol group with the ORD is highly conserved in Osh3 and Osh4, as suggested by good superposition of the head groups of the PI(4)P ligands (Figure 3C).

Conformational Change of ORD upon Ligand Binding

Structural comparison of apo- and PI(4)P-bound Osh3 ORD reveals that there is little conformational change upon ligand binding with an rmsd of 0.38 Å for all Cα atoms. The ligand-dependent conformational change is limited to several residues recognizing the head group of PI(4)P around the tunnel entrance and the small part of the lid (Figure 3D). There is almost no conformational change of the residues in the hydrophobic tunnel. In contrast, Osh4 undergoes a big conformational change upon sterol binding. Helix α7 (α8 in Osh3) moves its C terminus ~15 Å and the β1 strand and several loop regions near the tunnel

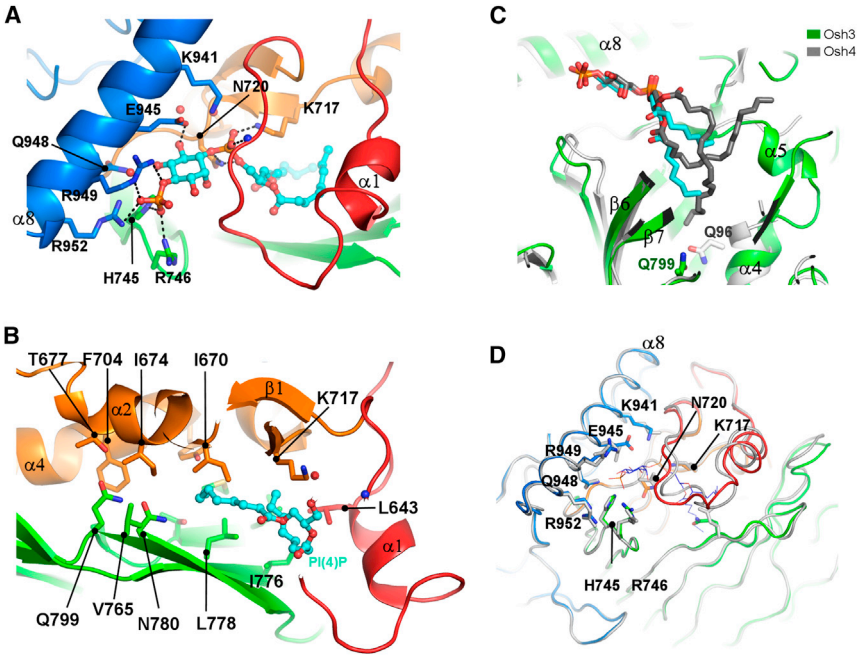

Figure 3. PI(4)P Binding to Osh3 ORD

(A) Binding of PI(4)P diC8 in the tunnel.

(B) The hydrophobic binding tunnel. The residues composing the wall of the hydrophobic tunnel are shown as ball-and-stick models.

(C) Comparison of PI(4)P recognition by Osh3 ORD and Osh4. Bound PI(4)P in Osh3 is cyan and the PI(4)P in Osh4 (PDB code 3SPW) is gray.

(D) Superposition of apo ORD and ORD-PI(4)P complex structures. The residues recognizing the PI(4)P head group are shown as ball-and-stick models.

See also Figures S1–S3.

opening move by up to 7 Å in Osh4. However, a conformational change of helix α8 in Osh3 is not possible due to the immobilization of the helix α8 by the C-terminal residues, Leu995 and Trp996, which are wedged between helices α7 and α8 (Figure S3A). The terminal hydrophobic residues (Leu-Trp) are well conserved in many long ORPs, implying that a big conformational change of helix α8 upon ligand binding is limited to only certain ORP members.

Osh3 Has no Sterol Binding Properties

OSBP was first discovered as a cytosolic receptor for oxysterols (Taylor et al., 1984), and sterol binding is a common theme in many ORPs. To examine the sterol binding property of Osh3, we performed in vitro ligand binding assays using recombinant Osh4 and Osh3 proteins (Figure 4A). The radioactive cholesterols alone or cholesterol-doped DOPC/PI(4)P liposomes were mixed with the purified Osh proteins. As previously reported, Osh4 showed good sterol binding. In contrast, all Osh3 constructs including full-length, PH-ORD, and ORD did not capture free cholesterols or extract cholesterols from the liposomes. To test whether Osh3 might selectively bind yeast sterols, a sterol extraction assay was performed using liposomes containing fluorescent dehydroergosterol (DHE), a natural ergosterol analog. Osh4 extracted DHE efficiently as monitored by a strong FRET signal between tryptophan residues and a bound DHE. Osh3 ORD did not extract DHE from the large DOPC liposomes of several different lipid compositions (Figures 4B and 4C). Consistent with in vitro binding assays, extensive cocrystallization trials to obtain sterol-bound Osh3 were not successful. Structure determination of the crystals grown in the presence of 10 mM sterols (ergosterol, cholesterol, 20-hydroxylcholesterol, or 25-hydroxycholesterol) showed empty binding pockets in the ORD. From these observations, we concluded that Osh3 does not bind sterols.

To gain a structural insight on the lack of sterol binding capacity of Osh3, we modeled a structure of ergosterol-bound Osh3 based on the structure of the Osh4-ergosterol complex. In Osh4, ergosterol binds to the central tunnel in a head-down orientation and the 3-hydroxyl group of the sterol is hydrogen-bonded to the side chain amide of Gln96 (α4) with a 2.7 Å distance (Im et al., 2005). The presence of the 3-hydroxyl group is a common feature of all sterol ligands and it is the only polar group in cholesterol and ergosterol. Despite the key feature of sterol ligands, Gln96 coordinating the 3-hydroxyl group is not conserved in all ORP homologs. In Osh3, Phe704 is present in the equivalent position to the Gln96 of Osh4. Instead, Gln799 of β10 is located within the hydrogen binding distance (3.0 Å) to the 3-hydroxyl group from the opposite direction to Phe704 in Osh3 (Figure 4D).

The careful inspection of the Osh3 ORD-ergosterol model revealed that the tunnel of Osh3 is too small to accommodate sterols. Even though the total volume of the ligand binding tunnel of Osh3 ORD is 3.5 times bigger than the volume of ergosterol (427.3 $Å^3$), the shape of the binding pocket is not compatible for sterol binding. The hydrophobic tunnel of Osh4 has a straight shape to fit the sterol molecule and provides enough room to contain a sterol and additional water molecules (Figure 4E). In contrast, the tunnel of Osh3 ORD is too narrow to accommodate the tetracyclic rings of sterol and is shorter than the long dimension of ergosterol (Figure 4F). Five residues of Osh3 are clashing with the modeled ergosterol in the binding pocket. Leu643 (α1), and Arg812 (β11) clashed with the side chain of ergosterol. Leu778 (β7), Asn780 (β7), and Tyr708 (α 4) clashed with the tetracyclic rings of ergosterol. The residues in the deep hydrophobic tunnel have little conformational changes upon sterol or PI(4)P binding in Osh4 and Osh3. Therefore, the possibility of sterol binding by an induced fit can be excluded in Osh3. Because ergosterol, cholesterol, and oxysterols share similar overall sizes and shapes, it is conceivable that sterols are not the ligands of Osh3.

The Residues Recognizing the PI(4)P Head Group Are Conserved in all ORDs

Structural comparison reveals that the overall structures of Osh3 ORD and sterol bound-Osh4 (PDB code: 1ZHZ) are

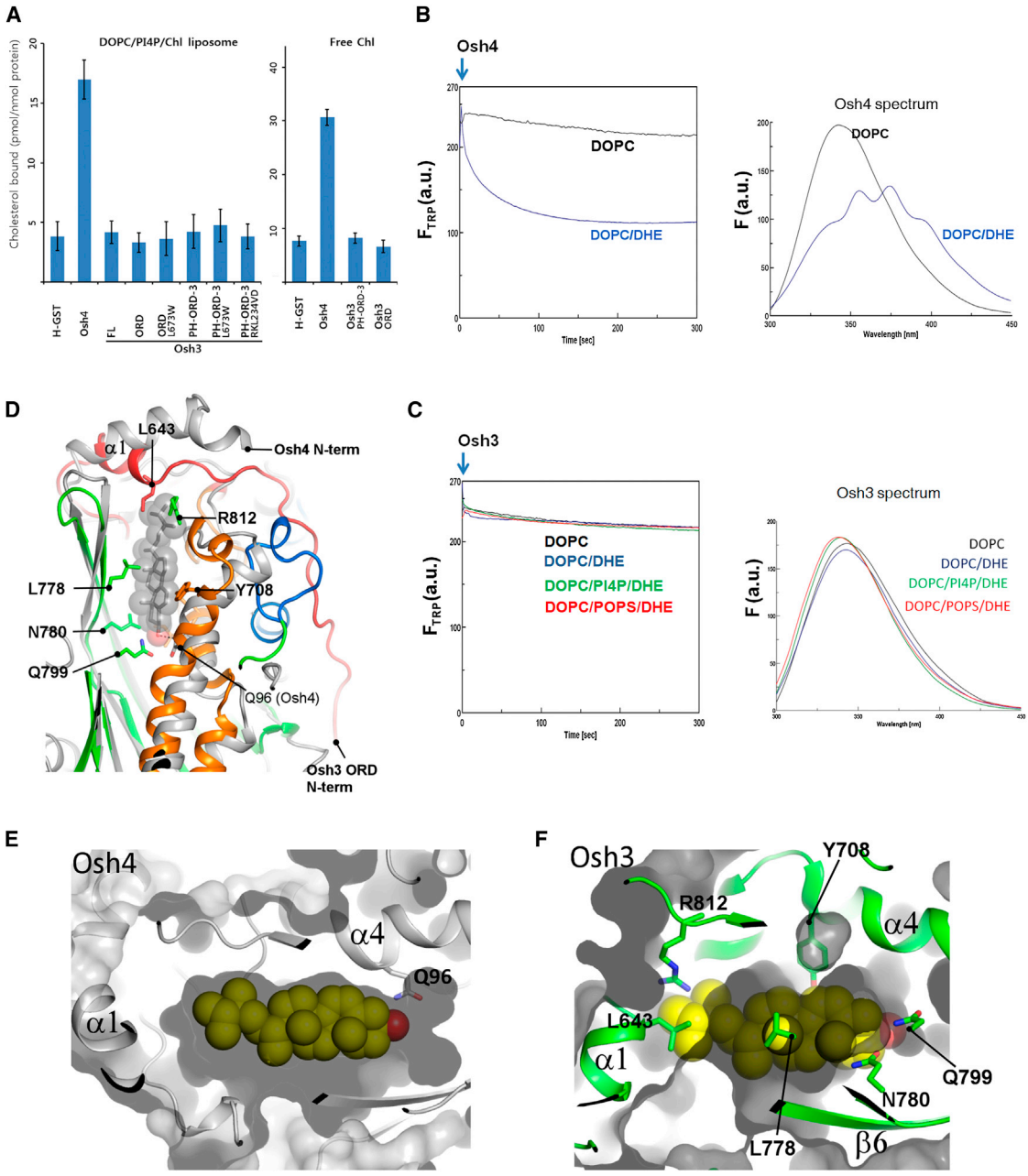

Figure 4. Measurement of Sterol Binding by Osh3 and Osh4

(A) Relative cholesterol binding affinities of Osh4 and various Osh3 constructs. The binding of radioactive cholesterol to Osh proteins immobilized to Ni-NTA beads was determined by scintillation counting as described in the Experimental Procedures. The error bars represent the SEs of the mean derived from the differences among the three measurements.

(B) Intrinsic fluorescence of Osh4 at 340 nm upon addition to DOPC/DHE (98:2 mol/mol) liposomes or to DOPC liposomes. Fluorescence emission spectra (λ_{ex} = 285 nm) of the samples at the end of the kinetics are shown on the right.

(C) Intrinsic fluorescence of Osh3 at 340 nm upon addition to various liposomes with different lipid compositions of DOPC, DOPC/DHE (98:2 mol/mol), DOPC/PI(4)P/DHE (97.5:0.5:2), or DOPC/POPS/DHE (88:10:2). Ten trytophan residues are in the Osh3 ORD and seven of them are within 20 Å from the ligand binding site.

(D) Structural comparison of the hydrophobic tunnels of Osh3 and Osh4. Ergosterol bound to Osh4 is shown as sticks with transparent spheres.

(E) Ergosterol binding in the hydrophobic tunnel of Osh4. Ergosterol is shown as a sphere model and Osh4 is shown in surface representation with backbones in ribbons.

(F) A model of ergosterol-bound Osh3 ORD. Osh3 is shown in surface representation. The residues clashing with the ergosterol are shown as sticks.

similar with a Cα rmsd of 1.53 Å for 205 equivalent residues out of 372 residues (Figure S3B). Osh3 ORD displays a compact structure with a smaller C-terminal subdomain than that of Osh4 (Figure S3C). The key residues involved in the recognition of the PI(4)P head group (Lys717, His745, Arg746, Lys943, Glu945, and Arg949) are strictly conserved in their amino acid

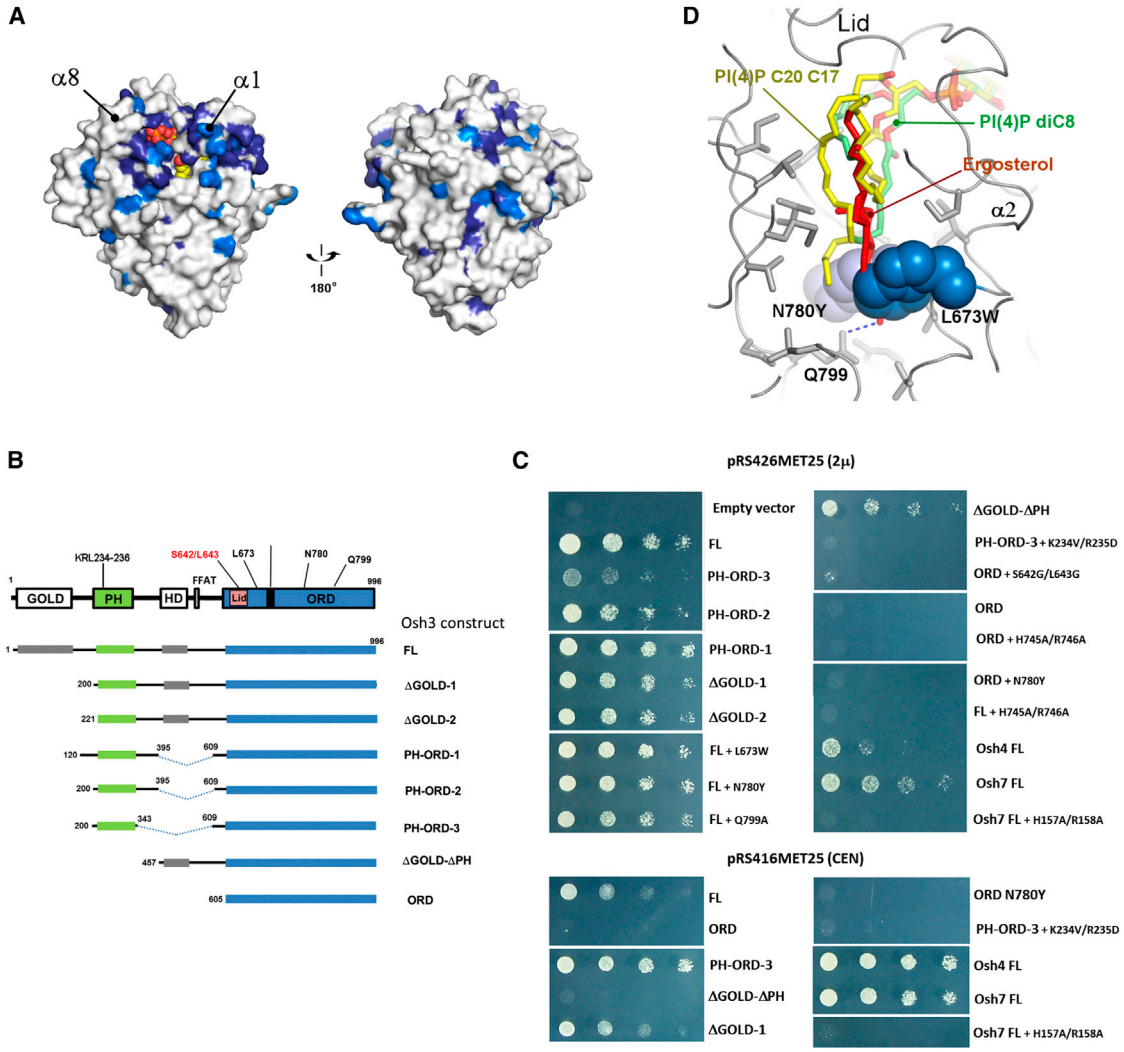

Figure 5. Yeast Complementation Analysis of Osh3 Constructs

(A) Surface representation of conserved residues. Conserved residues in six ORD homologs are blue and dark blue as shown in Figure S1.

(B) Schematic representation of the constructs used in this study. The sites of point mutations are indicated on top of the schematic representation. The internal loops that were deleted in PH-ORD constructs (indicated by dotted lines) were replaced by the TEV recognition sequence.

(C) Growth of *osh*Δ [*CEN osh4*^{ts}] cells coexpressing *OSH3*, *OSH4*, or *OSH7* alleles. Plasmids encoding Osh mutants were introduced into CBY926 yeast strains. The strains were grown at a permissive temperature (30°C), and the dilution series were incubated at 37°C.

(D) Effect of L673W and N780Y mutations on ligand binding. Ergosterol and PI(4)P C17 C20 were modeled into the hydrophobic tunnel of Osh3 ORD based on the structures of the Osh4-ligand complex. The conformation of the acyl chains of PI(4)P were slightly adjusted to fit into the pocket altered by N780Y and L673W mutations.

sequences and have almost identical conformations and geometries in Osh3 and Osh4. However, the acyl groups of PI(4)P have different conformations in the binding pockets. Many rotatable bonds in the acyl chains and nonspecific hydrophobic interactions within the binding tunnel might allow conformational flexibility of acyl chains of PI(4)P. Structural modeling suggests that PI(4)P molecules with various lengths of acyl chains up to C18 or C20 might be accepted in the binding pocket.

Osh3 ORD shows higher sequence homology to the ORDs of human ORPs than yeast Osh homologs. It displays high sequence homologies to the ORDs of ORP3 (51%), ORP7 (50%), ORP6 (49%), ORP2 (44%), and OSBP1 (43%). The surface representation of conserved residues of these ORP members showed that conservation of the tunnel entrance is a key feature of ORPs (Figure 5A). The strictly conserved residues are clustered in the binding site of the PI(4)P head group. In contrast, the residues in the deep hydrophobic pocket accommodating the acyl chains of PI(4)P or sterol molecules are not conserved. Even though the residues that recognize the 3-hydroxyl group of sterol molecules in Osh4 are not conserved, all ORP homologs have a cluster of polar residues at the bottom of the hydrophobic tunnel while the types and geometries of polar residues are variable. In Osh3, Tyr763, Thr677, Asn780, and Gln799 comprise the polar cluster at the tunnel bottom (Figure 3B).

Phosphoinositide Binding to PH and ORD Is Essential for Function

To assess the importance of individual domains of Osh3 for the biologic function, we tested whether the expression of various mutation and deletion constructs rescues the growth defects of a yeast strain in which all seven ORPs have either been deleted or are present as a temperature-sensitive allele (*osh⊿:CEN osh4^{ts}*; Beh et al., 2001). As expected, full-length Osh3 rescued cell growth at 37°C whereas the empty vector did not (Figures 5B and 5C). The N-terminal GOLD domain or FFAT motif was not essential for growth. ORD alone did not rescue the growth defects at 37°C. Addition of the PH domain to the ORD rescued the growth defects. The constructs in which the PH domain and ORD were connected by about 50 or 100 residues (constructs PH-ORD-3, -2, and -1) showed good viability. However, the KRL234-246VD mutation in the PH domain, which was expected to abolish phosphoinositide binding on the PH domain, was lethal. These results are consistent with the previous study that the PH domain is required for proper targeting of Osh3 to PM/ER contact sites (Stefan et al., 2011). Addition of an FFAT motif and the helical region to the ORD domain (constructs: ΔGOLD-ΔPH) rescued the growth in a 2μ plasmid (pRS426) but not in a single copy CEN plasmid (pRS416). These data suggest that a minimal requirement for Osh3 function is the presence of a targeting module such as the PH domain or FFAT motif to the ligand binding ORD.

We then examined the effect of mutations in the ligand binding pocket of the ORD. A mutation in the OSBP signature sequence (H745A/R746A) was lethal. Mutation of Gln799 to alanine, which was expected to abolish hydrogen bonding to the 3-hydroxyl group of the sterol ligand, still allowed growth of CBY926 cells. We assumed that the introduction of glycine residues to the lid (S642S/L643G) might increase the flexibility of the lid and lead to an enhanced uptake of ligands. However, S642G/L643G in full length and ORD constructs did not affect the growth of yeast cells. N780Y or L673W mutation on the hydrophobic wall in the binding tunnel did not abolish the growth of full-length Osh3. These mutations were expected to block the sterol binding by introducing bulky residues in the ligand binding tunnel. Structural modeling of the mutants revealed that the N780Y and L673W mutations hindered sterol binding by steric clash of the bulky residues with tetracyclic rings of sterols (Figure 5D). However, the mutations do not completely block the tunnel and still leave a space that can accommodate the acyl chains of PI(4)P. The two acyl chains of PI(4)P are mainly composed of single bonds. A slight adjustment of torsion angles of the acyl chain in the model allowed accommodation of PI(4)P in the hydrophobic tunnel of the mutants. These observations indicate that sterol binding is not an essential function of Osh3. In contrast, the mutations that abolished the recognition of PI(4)P were lethal, indicating that binding of phosphoinositide to the PH domain and ORD is essential for function.

Structural Modeling of Full-Length Osh3

A broad range of different membrane contacts sites (MCSs) is conserved across the entire range of eukaryotic cells. In budding yeast, the MCS distance between the PM and the peripheral ER ranges between 10 and 59 nm with a mean spacing of 33 nm (Levine, 2004; West et al., 2011). Because the major roles of ORPs were suggested to be lipid transfer proteins or regulators in closely apposed membranes, we checked whether the linear scale of individual domain separation is consistent with this concept. We built an extended linear model of full-length Osh3 using the PH and ORD structures determined in this study. The other regions were modeled as random loops based on the secondary structure prediction. The middle region connecting PH and ORD was modeled as random loops with an average Cα distance of 1.8 Å. The entire length between the PH domain and ORD in the extended conformation was ~59 nm, which covers the farthest MCS distance of 59 nm. The FFAT motif was separated from the PH domain by 37 nm and from ORD by 22 nm. Because each PH domain or the FFAT motif can be targeted to PM or ER by the association with PI(4)P in the PM or VAP proteins in the ER, this structural model is compatible with the concept that Osh3 can associate with two organellar membranes at the same time. The smallest PH-ORD constructs that were functional in the yeast complementation test had a distance of 9.2 nm between PH and ORD. Considering the flexibility of loops and the average Cα distance of 3.4 Å in an extended β strand conformation, the connecting loop is expected to cover maximally 1.8 times the distance represented in Figure 6. The modeling suggests that phosphoinositide sensing or transfer by Osh3 can be facilitated by the dual interactions of its N-terminal targeting domains with nearby membranes.

DISCUSSION

The crystal structures of Osh3 PH and ORD, together with biochemical and yeast complementation results, provide a detailed picture of a conserved ligand for ORDs and an important clue for the common function of the ORP family proteins. The N-terminal PH domain of Osh3 displays a classical PH domain fold with a highly basic phosphoinositide binding pocket. Osh3 ORD has a conserved β barrel fold with a ligand-binding tunnel in the center and the lid covering the tunnel entrance. The structural similarity of Osh3 and Osh4 suggests that the overall folding of ORDs might be well preserved among ORP members. Sequential and structural conservation of residues involved in the recognition of PI(4)P suggests that the binding of PI(4)P to ORDs is a general hallmark of the ORP family as proposed by the previous study on the Osh4 homolog (de Saint-Jean et al., 2011). Unlike the short ORP homolog Osh4, the upstream residues of the lid in Osh3 are tightly bound to the surface of the β barrel, which may prevent the tension between the N-terminal domains and ORD from affecting the conformation and gating of the lid.

Osh3 completely lacks sterol binding due to the narrow hydrophobic pocket. The absence of sterol binding activity in Osh3 is difficult to reconcile with the concept that Osh3 is a specific effector of sterol signaling or transport. Nonetheless, all ORPs have a polar cluster of hydrophilic residues at the bottom of the tunnel that may serve as hydrogen bonding partners to the 3-hydroxyl group of sterols or to other ligands. Variation in the residues and shapes of the binding pocket in ORPs suggests that sterol binding is specific to certain ORP members. Therefore, discovery of specific ligands other than PI(4)P to ORDs requires individual characterization of each ORP members.

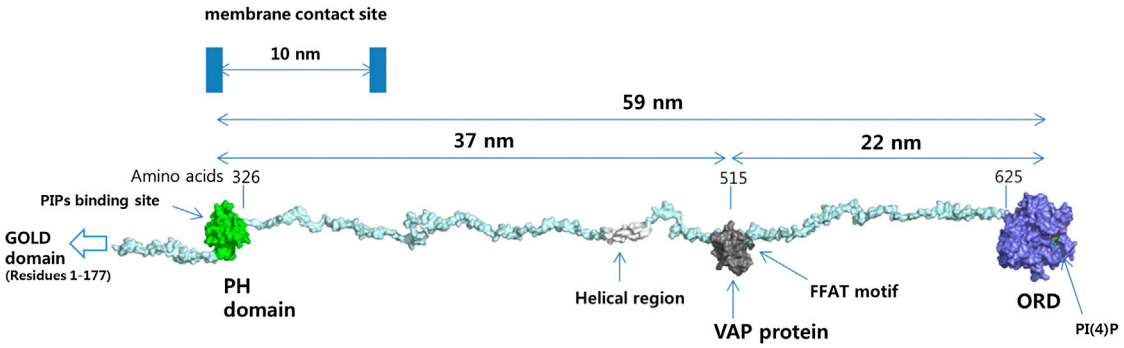

Figure 6. The Structural Model of Osh3

The linear structure of semi-full-length Osh3 was modeled based on the structures of the PH domain and ORD from this work. The structure of the VAP-FFAT motif was adapted from previous work (PDB code 1Z9O). The middle region (residues 326–625) between PH and ORD was modeled as partially extended loops with an average Cα distance of 1.8 Å between the residues. The N-terminal GOLD domain and the middle region in Osh3 were predicted to be mostly unstructured based on the secondary structure prediction (https://www.predictprotein.org/).

Nonvesicular lipid transport was suggested as one of the major functions of ORPs (Raychaudhuri et al., 2006; Schulz et al., 2009). A recent discovery of PI(4)P binding and transfer activity of Osh4 and OSBP1 suggested the role of ORPs as a sterol/PI(4)P exchanger (de Saint-Jean et al., 2011; Goto et al., 2012). ORP5 in the ER was known to be involved in cholesterol trafficking in endosomes and lysosomes (Du et al., 2011). It has been proposed that lipid transport proteins might work more efficiently at membrane contacts sites because they have to diffuse only a short distance between membranes (Hanada et al., 2007). The structural model of Osh3 is fully compatible with the role as lipid transfer proteins at the closely apposed membrane contact sites. The PH domain and FFAT motif might help with the proper targeting of Osh3 to the MCSs of PM and ER and the ORD might transport PI(4)P by uptake or release of the lipid from the membranes. Osh proteins (Osh3–Osh7) are known to act as controllers of PI(4)P signaling and metabolism by regulating Sac1 phosphatase activity at the MCSs (Stefan et al., 2011). It is probable that the Osh3 or other Osh homologs might sense the PI(4)P level in the plasma membrane by extracting the lipid into the ORD and might regulate Sac1 activity by the Sac1-ORD interaction. Despite the common PI(4)P binding by Osh proteins, domain architectures of Osh homologs (Osh3, Osh4, and Osh7) are distinct and the conservation of surface residues is limited to the tunnel entrance. In addition, the small conformational change of Osh3 ORD upon PI(4)P binding is limited to a few residues involved in PI(4)P recognition while extensive conformational changes are involved in Osh4. The poor overall consensus of ligand-induced conformational changes between Oshs contrasts to the shared role of Osh proteins on Sac1 regulation. Perhaps the Sac1 regulation might involve direct recognition of the bound PI(4)P and the conserved OSBP fingerprint motif by Sac1. Simple alternative interpretation would be that the increase of phosphatase activity of Sac1 by Osh proteins is mediated by substrate presentation by ORDs. Osh proteins as lipid transfer proteins might extract PI(4)P from the plasma membrane and present it to Sac1 phosphatase or transport the substrates to the membrane, where the catalytic domain of Sac1 phosphatase is located. Two models do not seem to exclude each other, because PI(4)P sensing by ligand uptake and release might be coupled to the lipid transfer cycles. To obtain the accurate mechanistic understanding of Sac1 regulation by Osh proteins, further biochemical and structural studies are required.

Seven Osh homologs in yeast share at least one essential function, which was proposed from the observation that introduction of any one of the *OSH* alleles makes the seven Osh deletion strain viable (Beh and Rine, 2004). The expression of human ORP1 rescues the inviability of Osh-deficient yeast cells, indicating that the essential role of ORPs is shared even between species (Fairn and McMaster, 2008). Analysis of all *OSH* deletion combinations identified two viable strains, *osh⊿ OSH1 OSH3* and *osh⊿ OSH3 OSH6,* in which the sterol distribution differed from that in the wild-type (Beh et al., 2001). These strains have defects in the maintenance of normal sterol levels in the PM and display abnormal accumulation of sterols in internal membranes. In addition, the phenotypic effect of single deletions on yeast cells was greatest in the *OSH4/KES1* deletion and was least in the *OSH3* deletion (Beh et al., 2001). Our work explains these observations in that Osh3 completely lacks sterol binding capacity. Because Osh3 rescues the *OSH1-7* deletion strain, sterol regulation by Osh proteins can be excluded from the essential function. This proposal is supported by the observation that the N780Y mutation that blocks the sterol binding pocket without interfering with PI(4)P binding was still viable. The Y97F mutation in Osh4 disrupts sterol association but the allele is not a loss-of-function mutation, suggesting a nonessential role of sterol binding in the ORP family (Im et al., 2005). Osh proteins regulate membrane sterol organization but are not essential for sterol movement between the ER and PM in yeast (Georgiev et al., 2011). In addition, several Osh homologs (Osh1, Osh6, and Osh7) have poor sterol transfer activity in vitro, implying that lack of sterol binding might not be limited to the Osh3 homolog (Schulz et al., 2009). In contrast, any mutations that abolish PI(4)P recognition in Osh3 ORD, Osh4, or Osh7 were lethal, confirming that PI(4)P regulation is central to common essential function.

Although ORPs share an essential role between homologs, the cellular functions of each homolog are diverse. Some ORPs may act as lipid sensors and regulate other proteins in response to sterol binding, implying that ORPs have a specific role in addition to the conserved essential role. The major challenge for the

future will be to unravel whether the diverse roles of ORPs in cell signaling and sterol trafficking have a direct relationship with the conserved role in PI(4)P regulation or represent distinct aspects of ORP function.

In summary, the results described here provide a clear-cut validation for the conservation of phosphoinositide binding to ORDs. The strictly conserved "OSBP fingerprint motif" EQVSHHPP turned out to be a specific binding motif for the head group of PI(4)P ligand, redefining the major role of OSBPs as phosphoinositide binding proteins. The structures at up to 1.5 Å resolution provide details of the shape of ORD from long ORP members and should be an important addition to the structural understanding of the diverse roles of ORP proteins.

EXPERIMENTAL PROCEDURES

Crystallization and Crystallographic Analysis

Crystals of Osh3 PH-T4L and apo Osh3 ORD were grown as described (Tong et al., 2012). For the crystallization of the Osh3 ORD-PI(4)P complex, purified Osh3 ORD was mixed with soluble PI(4)P diC8 at a 1:2 molar ratio and was incubated at room temperature for 2 hr. The complex was crystallized in 0.1 M MES-NaOH pH 6.0, 25% PEG 1500, and 0.1 M $MgCl_2$. Osh3 PH-T4L crystallized in space group C2 with two copies in the asymmetric unit and a solvent content of 0.61. Native data sets of Osh3 PH-lysozyme were collected at a wavelength of 0.97949Å at the PLS 5C beamline. The structure of Osh3 PH-T4L was determined by molecular replacement using the structure of T4 lysozyme (PDB code: 212L). Two molecules of T4 lysozyme were found in the asymmetric unit using the program MOLREP (Vagin and Teplyakov, 2010) and the density-modified map showed clear electron densities of the PH domains. The final model including two molecules of Osh3 PH-T4L, eight sulfate ions, and 106 water molecules was refined to R_{work}/R_{free} values of 24.4%/27.6%. Diffraction data for native Osh3 ORD were collected at a fixed wavelength of 0.91997 Å using at the SSRF BL17U1 beamline. For structure determination, Br SAD data sets were collected using bromine labeled crystals at the peak wavelength of 0.91950 Å at the Photon Factory AR-NW12A beamline. SAD phasing was performed with the program SOLVE and density modification was done using RESOLVE (Terwilliger and Berendzen, 1999). The resulting electron density map with a figure of merit of 0.67 was readily interpretable. After model building, the structure of apo-ORD was refined against the native data set to final R_{work}/R_{free} values of 21.3%/23.9%, respectively at 1.5 Å resolution. Diffraction data for the Osh3 ORD-PI(4)P complex were collected at a fixed wavelength of 0.97949 Å at the PLS 5C beamline. The structure was determined by molecular replacement using the structure of apo-Osh3 ORD. The bound PI(4)P molecule was clearly visible in the 2Fo-Fc map (Figure S3). The model was refined to R_{work}/ R_{free} values of 23.2%/28.0% at 2.2 Å resolution.

Liposomes

DOPC (1, 2-dioleoyl-*sn*-glycero-3-phosphocholine), POPS (1-palmitoyl-2-oleoyl-*sn*-glycero-3-phospho-l-serine), and PI(4)P from porcine brain were obtained from Avanti Polar Lipids. Ergosterol and DHE were obtained from Sigma-Aldrich. Radioactive [^{3}H] cholesterol was purchased from American Radiolabeled Chemicals. Lipids in stock solutions in chloroform or in ethanol were mixed at the desired molar ratio, incubated at 37°C for 5 min, and the solvent was evaporated by nitrogen stream. Dried lipids were resuspended in 50 mM HEPES pH 7.2, and 120 mM potassium acetate (HK buffer) by vortexing. Liposomes were prepared at a total lipid concentration of 0.76 mg/ml. The hydrated lipid mixture was frozen and thawed five times using a water bath and cooled ethanol at −70°C. The lipid mixture was extruded ten times through a 0.1 μm (pore size) polycarbonate filter. The liposomes were diluted two times with HK buffer to the final lipid concentration of 0.5 mM. The liposomes were stored at 4°C in the dark and used within 3 days.

[^{3}H]-Cholesterol Binding Assay

Various His-GST-tagged Osh3 and Osh4 proteins were expressed in *E. coli* strain BL21(DE3). After cell lysis, the proteins in the supernatants were captured by Ni^{2+}-NTA beads. The Osh protein loaded Ni^{2+}-NTA beads were washed with 2× PBS containing 20 mM imidazole. Two hundred microliters of liposomes (molar ratio DOPC: PI[4]P: cholesterol = 96:3:1) containing 0.1 μCi/ml of radioactive cholesterol was added to 30 μl of Osh3-loaded Ni^{2+}-NTA beads at a final lipid concentration of 0.5 mM. The Osh protein-liposome mixture was incubated for 30 min at room temperature. For the binding assay of free sterols, 50 pmol of radioactive cholesterol solubilized in ethanol was mixed with Osh3-loaded Ni^{2+}-NTA beads. The unbound radioactive cholesterols were washed using 2× PBS buffer containing 1% Triton X-100 three times. The fusion protein was eluted by an elution buffer containing 0.1 M Tris pH 8.0, 0.3 M NaCl, and 0.3 M imidazole. The radioactivity of the eluate was measured with a scintillation counter. To estimate the nonspecific binding of cholesterol, Ni-NTA beads loaded with His-GST were used as negative controls. The experiment was repeated three times.

DHE Loading Assay

A fluorescence-based DHE loading assay was adopted from a recent report (de Saint-Jean et al., 2011). For kinetics measurements, Trp fluorescence was measured at 340 nm (bandwidth 5 nm) upon excitation at 285 nm (bandwidth 5 nm) in a fluorometer (FP-6200; JASCO). One milliliter of the sample that initially contained liposomes (1 mM total lipids) was diluted two times with HK buffer. The sample (volume 2 ml) was placed in a square quartz cell and continuously stirred with a small magnetic bar at room temperature. Osh4 or Osh3 proteins were injected from stock solution to the sample cell with a final protein concentration of 0.5 μM; kinetic measurements started instantly. Emission spectra were recorded at the end of the kinetics upon excitation at 285 nm.

Plasmid Construction and Yeast Strains

DNA coding for the genes for *OSH3* were amplified from yeast genomic DNA and cloned to pRS426MET25 or pRS416MET25. Mutant constructs were generated by site-directed mutagenesis and confirmed by DNA sequencing. Plasmids encoding the *OSH3* gene were transformed to the CYB926 strain. Complementation analysis was performed by introducing the plasmids encoding mutant Osh3 proteins into the CBY926 strain (*Osh1–7Δ:CEN osh4^{ts}*) (Beh and Rine, 2004). The transformed cells were grown at 30°C and the serial dilutions of cells were incubated at 37°C.

ACCESSION NUMBERS

The PDB accession numbers for the coordinates and structure factors of Osh3 PH-T4L, apo Osh3 ORD, and the Osh3 ORD-PI(4)P complex are 4IAP, 4IC4, and 4INQ, respectively.

SUPPLEMENTAL INFORMATION

Supplemental Information includes Supplemental Experimental Procedures, three figures, and two 3D molecular models and can be found with this article online at http://dx.doi.org/10.1016/j.str.2013.05.007.

ACKNOWLEDGMENTS

We appreciate C. Beh for providing the yeast CYB926 strain. This research was supported by the Basic Science Research Program through the National Research Foundation of Korea (NRF), funded by the Ministry of Education, Science and Technology (grant nos. NRF-2010-0013448 and NRF-2011-0025110).

Received: January 21, 2013
Revised: April 25, 2013
Accepted: May 8, 2013
Published: June 20, 2013

REFERENCES

Baumann, N.A., Sullivan, D.P., Ohvo-Rekilä, H., Simonot, C., Pottekat, A., Klaassen, Z., Beh, C.T., and Menon, A.K. (2005). Transport of newly synthesized sterol to the sterol-enriched plasma membrane occurs via nonvesicular equilibration. Biochemistry *44*, 5816–5826.

Beh, C.T., and Rine, J. (2004). A role for yeast oxysterol-binding protein homologs in endocytosis and in the maintenance of intracellular sterol-lipid distribution. J. Cell Sci. *117*, 2983–2996.

Beh, C.T., Cool, L., Phillips, J., and Rine, J. (2001). Overlapping functions of the yeast oxysterol-binding protein homologues. Genetics *157*, 1117–1140.

Beh, C.T., McMaster, C.R., Kozminski, K.G., and Menon, A.K. (2012). A detour for yeast oxysterol binding proteins. J. Biol. Chem. *287*, 11481–11488.

de Saint-Jean, M., Delfosse, V., Douguet, D., Chicanne, G., Payrastre, B., Bourguet, W., Antonny, B., and Drin, G. (2011). Osh4p exchanges sterols for phosphatidylinositol 4-phosphate between lipid bilayers. J. Cell Biol. *195*, 965–978.

Du, X., Kumar, J., Ferguson, C., Schulz, T.A., Ong, Y.S., Hong, W., Prinz, W.A., Parton, R.G., Brown, A.J., and Yang, H. (2011). A role for oxysterol-binding protein-related protein 5 in endosomal cholesterol trafficking. J. Cell Biol. *192*, 121–135.

Fairn, G.D., and McMaster, C.R. (2008). Emerging roles of the oxysterol-binding protein family in metabolism, transport, and signaling. Cell. Mol. Life Sci. *65*, 228–236.

Georgiev, A.G., Sullivan, D.P., Kersting, M.C., Dittman, J.S., Beh, C.T., and Menon, A.K. (2011). Osh proteins regulate membrane sterol organization but are not required for sterol movement between the ER and PM. Traffic *12*, 1341–1355.

Goto, A., Liu, X., Robinson, C.A., and Ridgway, N.D. (2012). Multi-site phosphorylation of oxysterol binding protein (OSBP) regulates sterol binding and activation of Sphingomyelin synthesis. Mol Biol Cell *23*, 3624–3635.

Hanada, K., Zhang, X., Borevitz, J.O., Li, W.H., and Shiu, S.H. (2007). A large number of novel coding small open reading frames in the intergenic regions of the Arabidopsis thaliana genome are transcribed and/or under purifying selection. Genome Res. *17*, 632–640.

Im, Y.J., Raychaudhuri, S., Prinz, W.A., and Hurley, J.H. (2005). Structural mechanism for sterol sensing and transport by OSBP-related proteins. Nature *437*, 154–158.

Kozminski, K.G., Alfaro, G., Dighe, S., and Beh, C.T. (2006). Homologues of oxysterol-binding proteins affect Cdc42p- and Rho1p-mediated cell polarization in Saccharomyces cerevisiae. Traffic *7*, 1224–1242.

Lehto, M., Laitinen, S., Chinetti, G., Johansson, M., Ehnholm, C., Staels, B., Ikonen, E., and Olkkonen, V.M. (2001). The OSBP-related protein family in humans. J. Lipid Res. *42*, 1203–1213.

Lessmann, E., Ngo, M., Leitges, M., Minguet, S., Ridgway, N.D., and Huber, M. (2007). Oxysterol-binding protein-related protein (ORP) 9 is a PDK-2 substrate and regulates Akt phosphorylation. Cell. Signal. *19*, 384–392.

Levine, T. (2004). Short-range intracellular trafficking of small molecules across endoplasmic reticulum junctions. Trends Cell Biol. *14*, 483–490.

Levine, T.P., and Munro, S. (2001). Dual targeting of Osh1p, a yeast homologue of oxysterol-binding protein, to both the Golgi and the nucleus-vacuole junction. Mol. Biol. Cell *12*, 1633–1644.

Loewen, C.J., Roy, A., and Levine, T.P. (2003). A conserved ER targeting motif in three families of lipid binding proteins and in Opi1p binds VAP. EMBO J. *22*, 2025–2035.

Mesmin, B., and Maxfield, F.R. (2009). Intracellular sterol dynamics. Biochim. Biophys. Acta *1791*, 636–645.

Mesmin, B., Antonny, B., and Drin, G. (2013). Insights into the mechanisms of sterol transport between organelles. Cellular and molecular life sciences. Cell. Mol. Life Sci. http://dx.doi.org/10.1007/s00018-012-1247-3

Ngo, M.H., Colbourne, T.R., and Ridgway, N.D. (2010). Functional implications of sterol transport by the oxysterol-binding protein gene family. Biochem. J. *429*, 13–24.

Raychaudhuri, S., and Prinz, W.A. (2010). The diverse functions of oxysterol-binding proteins. Annu. Rev. Cell Dev. Biol. *26*, 157–177.

Raychaudhuri, S., Im, Y.J., Hurley, J.H., and Prinz, W.A. (2006). Nonvesicular sterol movement from plasma membrane to ER requires oxysterol-binding protein-related proteins and phosphoinositides. J. Cell Biol. *173*, 107–119.

Ridgway, N.D., Dawson, P.A., Ho, Y.K., Brown, M.S., and Goldstein, J.L. (1992). Translocation of oxysterol binding protein to Golgi apparatus triggered by ligand binding. J. Cell Biol. *116*, 307–319.

Schulz, T.A., Choi, M.G., Raychaudhuri, S., Mears, J.A., Ghirlando, R., Hinshaw, J.E., and Prinz, W.A. (2009). Lipid-regulated sterol transfer between closely apposed membranes by oxysterol-binding protein homologues. J. Cell Biol. *187*, 889–903.

Stefan, C.J., Manford, A.G., Baird, D., Yamada-Hanff, J., Mao, Y., and Emr, S.D. (2011). Osh proteins regulate phosphoinositide metabolism at ER-plasma membrane contact sites. Cell *144*, 389–401.

Taylor, F.R., Saucier, S.E., Shown, E.P., Parish, E.J., and Kandutsch, A.A. (1984). Correlation between oxysterol binding to a cytosolic binding protein and potency in the repression of hydroxymethylglutaryl coenzyme A reductase. J. Biol. Chem. *259*, 12382–12387.

Terwilliger, T.C., and Berendzen, J. (1999). Evaluation of macromolecular electron-density map quality using the correlation of local r.m.s. density. Acta Crystallogr. D Biol. Crystallogr. *55*, 1872–1877.

Tong, J., Yang, H., Ha, S., Lee, Y., Eom, S.H., and Im, Y.J. (2012). Crystallization and preliminary X-ray crystallographic analysis of the oxysterol-binding protein Osh3 from Saccharomyces cerevisiae. Acta Crystallogr. Sect. F Struct. Biol. Cryst. Commun. *68*, 1498–1502.

Vagin, A., and Teplyakov, A. (2010). Molecular replacement with MOLREP. Acta Crystallogr. D Biol. Crystallogr. *66*, 22–25.

Vihervaara, T., Jansen, M., Uronen, R.L., Ohsaki, Y., Ikonen, E., and Olkkonen, V.M. (2011a). Cytoplasmic oxysterol-binding proteins: sterol sensors or transporters? Chem. Phys. Lipids *164*, 443–450.

Vihervaara, T., Uronen, R.L., Wohlfahrt, G., Björkhem, I., Ikonen, E., and Olkkonen, V.M. (2011b). Sterol binding by OSBP-related protein 1L regulates late endosome motility and function. Cell. Mol. Life Sci. *68*, 537–551.

Wang, P.Y., Weng, J., and Anderson, R.G. (2005). OSBP is a cholesterol-regulated scaffolding protein in control of ERK 1/2 activation. Science *307*, 1472–1476.

West, M., Zurek, N., Hoenger, A., and Voeltz, G.K. (2011). A 3D analysis of yeast ER structure reveals how ER domains are organized by membrane curvature. J. Cell Biol. *193*, 333–346.

Yu, J.W., Mendrola, J.M., Audhya, A., Singh, S., Keleti, D., DeWald, D.B., Murray, D., Emr, S.D., and Lemmon, M.A. (2004). Genome-wide analysis of membrane targeting by S. cerevisiae pleckstrin homology domains. Mol. Cell *13*, 677–688.

Structure, Volume *21*

Supplemental Information

Structure of Osh3 Reveals a Conserved Mode of Phosphoinositide Binding in Oxysterol-Binding Proteins

Junsen Tong, Huiseon Yang, Hongyuan Yang, Soo Hyun Eom, and Young Jun Im

Inventory of Supplemental Information

Figures

Experimental procedures

PH domains

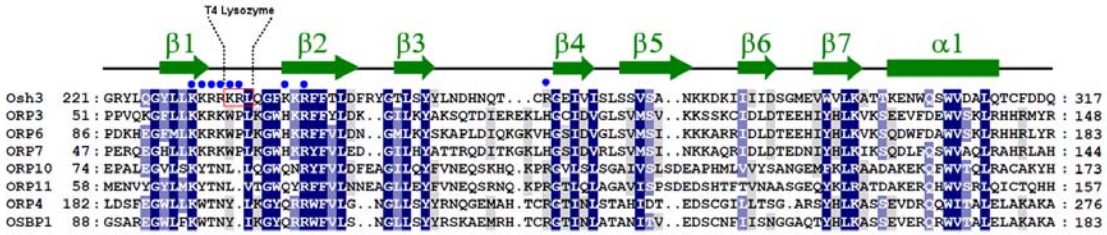

ORD domains

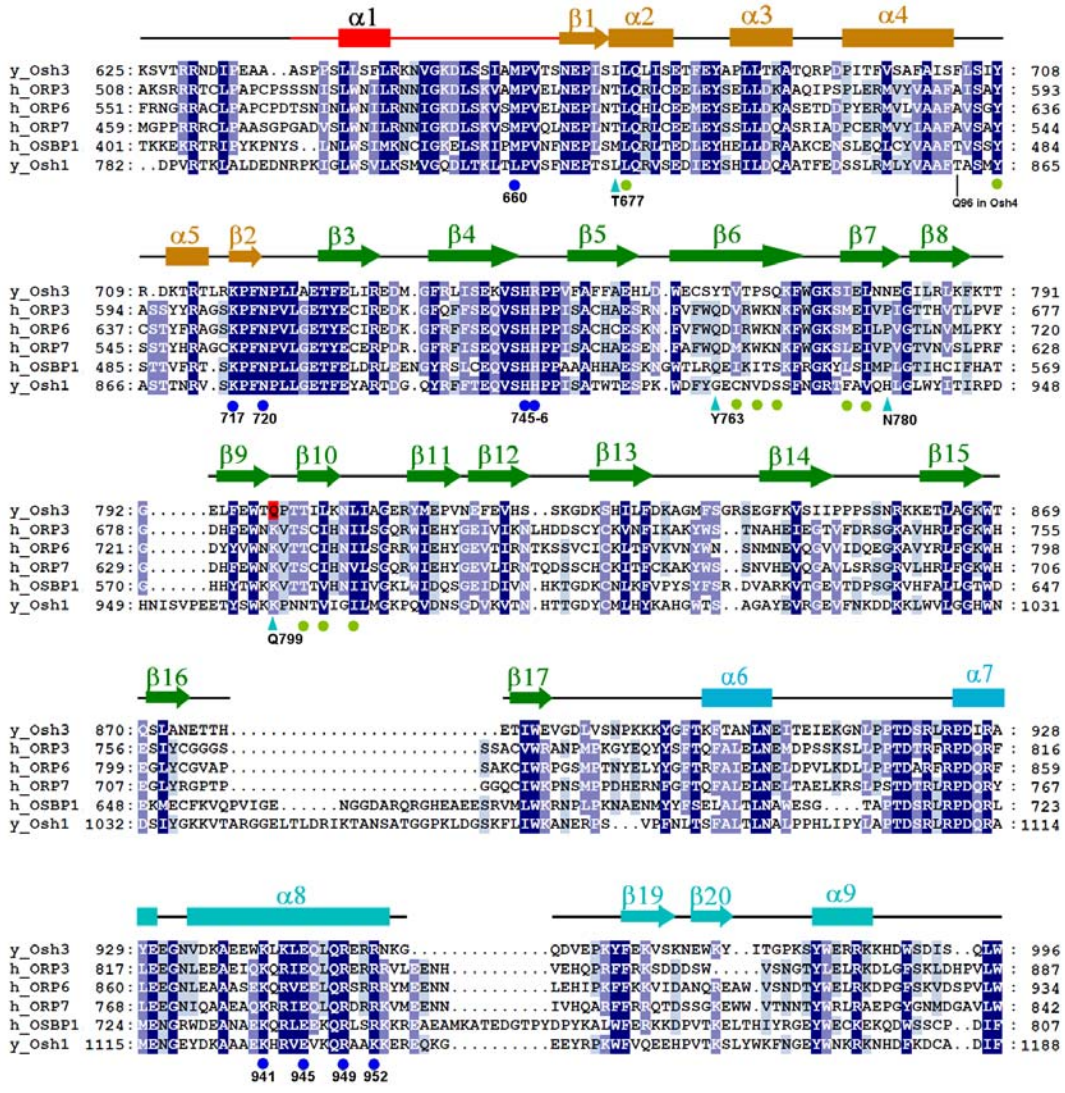

Figure S1. Sequence alignment of Osh homologs

Amino acids sequences of PH domains and ORDs from yeast and human ORPs were aligned using the program ClustalX. Four human ORPs and yeast Osh1 displaying high sequence homologies to Osh3 and were selected for analysis. Conserved residues are colored in dark blue, blue, and light blue, according to their respective degree of conservation from highest to lowest. The basic residues on the phosphoinoside binding surface of the PH domain were marked with blue dots. The conserved residues in the ORD recognizing the head group of PI(4)P ligand are indicated as blue dots. The residues on the wall of the hydrophobic tunnel are shown as green dots. Polar residues at the bottom of the tunnel are indicated as cyan triangles.

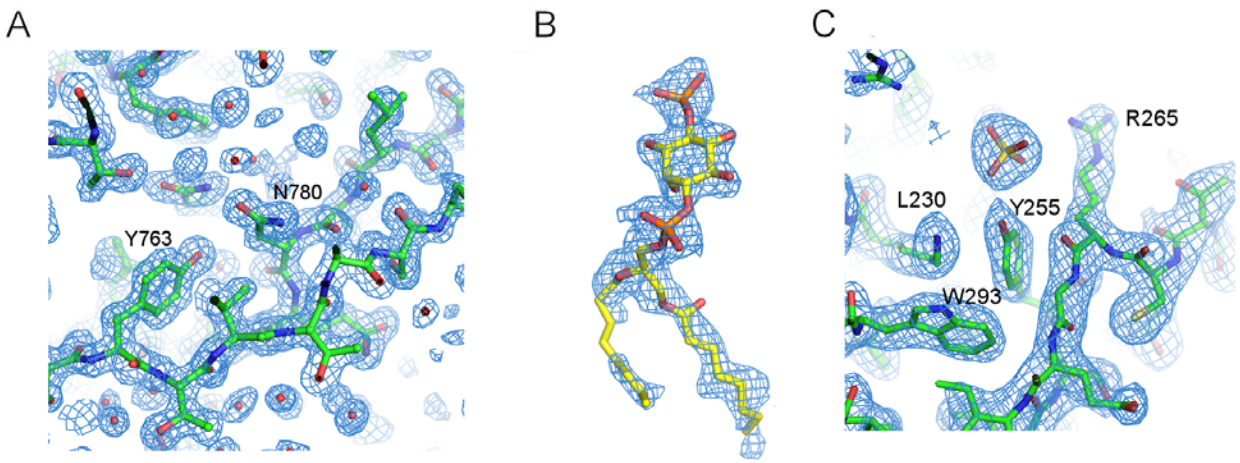

Figure S2. Electron density maps

(A) The 1.5 Å 2Fo-Fc composite annealed omit map of apo Osh3 ORD with the final model superimposed.

(B) The 2.2 Å simulated annealing omit map of PI(4)P ligand in the Osh3 ORD-PI(4)P complex with the final model superimposed.

(C) The 2.3 Å 2Fo-Fc composite annealed omit map of Osh3 PH with the final model superimposed.

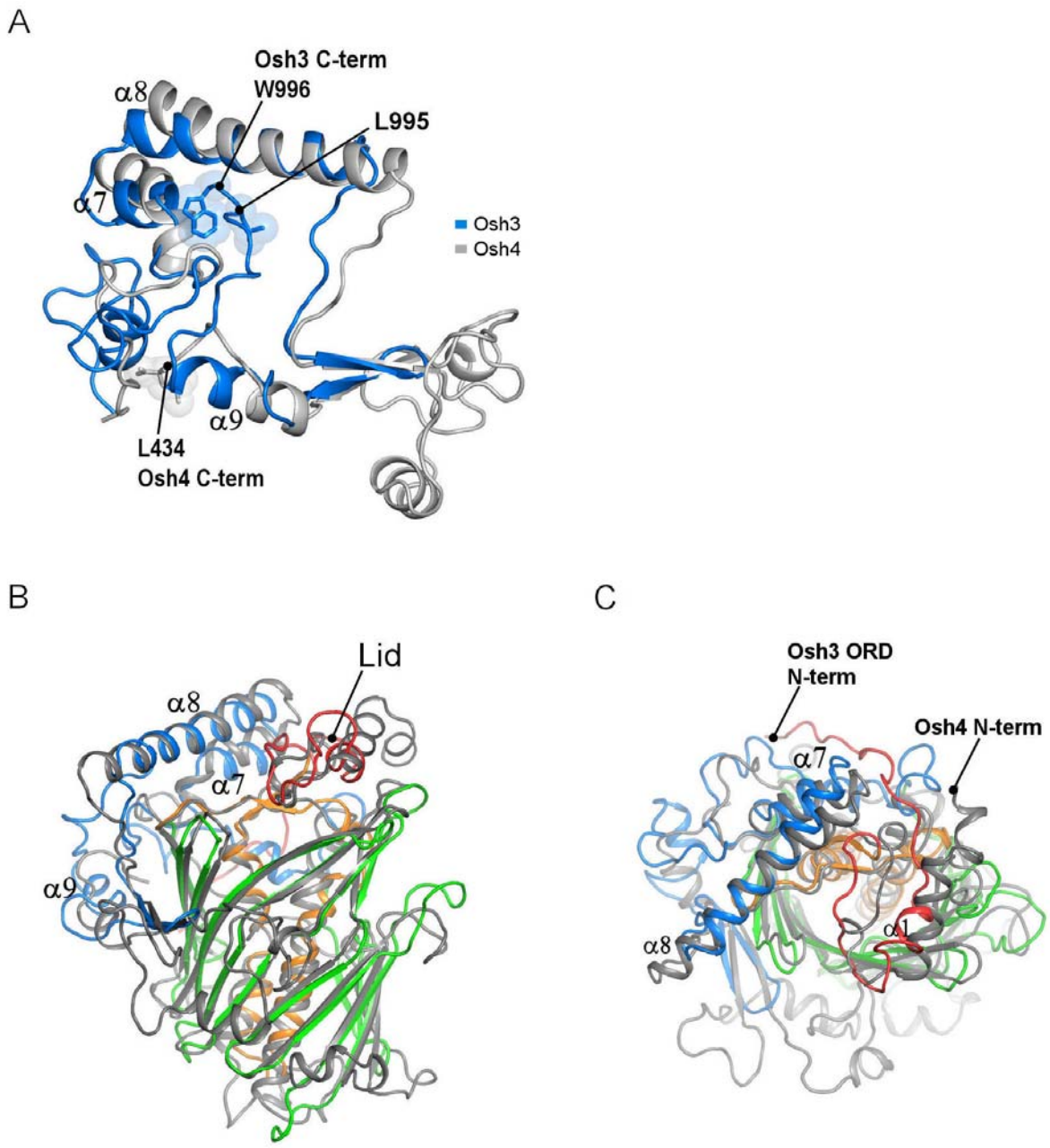

Figure S3. Structural comparison of Osh3 and Osh4

(A) The superposition of the C-terminal subdomains from Osh3 and Osh4. Osh3 is shown in red and Osh4 in gray. The C-terminal two amino acids of Osh3, Trp996 and Leu995, are shown in sticks.

(B) The structures of Osh3 ORD and Osh4 (PDB code: 1ZHT) were superimposed for comparison. Osh3 is shown in a color scheme as in Figure 2A and Osh4 is shown in gray.

(C) Top view of the superimposed structures in Figure S4B.

Protein expression and purification

Details of protein expression and crystallographic procedures were described elsewhere (Tong et al., 2012). Briefly describing, DNA encoding the PH domain (residues 221-317) was subcloned into a pHIS-2 vector providing a cleavable N-terminal His tag by thrombin protease. To increase the solubility of the PH domain construct and to facilitate structure determination by molecular replacement, a tripeptide (KRL) in the loop β1-β2 (residues 234-236) was replaced by bacteriophage T4 lysozyme (residues 2 - 161). Osh3 ORD (residues 605-996) was subcloned into a modified pGEX-4T vector providing a cleavable His-GST tag by TEV protease. *Escherichia coli* strain BL21(DE3) transformed with the plasmids encoding the PH domain or ORD were grown at 310 K in LB medium and the cells were induced by adding 0.5 m*M* IPTG. His-PH-T4L was purified by Ni-NTA affinity chromatography. The eluted protein was concentrated to 10 mg/ml and the His-tag was removed by cleavage with thrombin protease. Subsequently, the sample was subjected to size exclusion chromatography on a Superdex 200 column equilibrated with 20 m*M* Tris-HCl (pH 8.0), 300 m*M* NaCl, and 10 m*M* β-mercaptoethanol. Fractions containing the PH-T4L were concentrated to 12 mg/ml for crystallization. His-GST-ORD was initially purified by Ni-NTA affinity chromatography and the His-GST tag was removed by cleavage with TEV protease. The Osh3 ORD was separated from His-GST by HiTrap SP ion exchange chromatography. Osh3 ORD was subjected to size exclusion chromatography on a Superdex 200 column equilibrated with 20 m*M* Tris-HCl (pH 8.0), 150 m*M* NaCl. The fractions containing the Osh3 ORD were concentrated to 10 mg/ml for crystallization. DNAs encoding various portions of Osh3 were cloned to the modified pGEX-4T vector providing an N-terminal His-GST tag with a thrombin cleavage sequence. The expression and purification of full length

Osh3 and other domains were carried out using the same procedure used for the Osh3 PH-T4L construct.

References

Tong, J., Yang, H., Ha, S., Lee, Y., Eom, S.H., and Im, Y.J. (2012). Crystallization and preliminary X-ray crystallographic analysis of the oxysterol-binding protein Osh3 from Saccharomyces cerevisiae. Acta crystallographica Section F, Structural biology and crystallization communications *68*, 1498-1502.